ACS Chemical Neuroscience

Research Article

pubs.acs.org/chemneuro

ML297 (VU0456810), the First Potent and Selective Activator of the GIRK Potassium Channel, Displays Antiepileptic Properties in Mice

Kristian Kaufmann,[‡] Ian Romaine,[†,§] Emily Days,[†] Conrado Pascual,[▽] Adam Malik,[▽] Liya Yang,[▽] Bende Zou,[▽] Yu Du,[‡] Greg Sliwoski,[‡] Ryan D. Morrison,[∥,#] Jerod Denton,[‡,⊥] Colleen M. Niswender,[‡,#] J. Scott Daniels,[‡,∥,#] Gary A. Sulikowski,[†,§] Xinmin (Simon) Xie,[▽] Craig W. Lindsley,[†,‡,§,∥,#] and C. David Weaver*[,†,‡]

[†]Vanderbilt Institute of Chemical Biology, [‡]Department of Pharmacology, [§]Department of Chemistry, [∥]Vanderbilt Specialized Chemistry Center, [⊥]Division of Anesthesiology, and [#]Vanderbilt Center for Neuroscience Drug Discovery, Vanderbilt University, Nashville, Tennessee 37232, United States

[▽]AfaSci Research Laboratory, Redwood City, California 94063, United States

Supporting Information

ABSTRACT: The G-protein activated, inward-rectifying potassium (K^+) channels, "GIRKs", are a family of ion channels ($K_{ir}3.1$-$K_{ir}3.4$) that has been the focus of intense research interest for nearly two decades. GIRKs are comprised of various homo- and heterotetrameric combinations of four different subunits. These subunits are expressed in different combinations in a variety of regions throughout the central nervous system and in the periphery. The body of GIRK research implicates GIRK in processes as diverse as controlling heart rhythm, to effects on reward/addiction, to modulation of response to analgesics. Despite years of GIRK research, very few tools exist to selectively modulate GIRK channels' activity and until now no tools existed that potently and selectively activated GIRKs. Here we report the development and characterization of the first truly potent, effective, and selective GIRK activator, ML297 (VU0456810). We further demonstrate that ML297 is active in two in vivo models of epilepsy, a disease where up to 40% of patients remain with symptoms refractory to present treatments. The development of ML297 represents a truly significant advancement in our ability to selectively probe GIRK's role in physiology as well as providing the first tool for beginning to understand GIRK's potential as a target for a diversity of therapeutic indications.

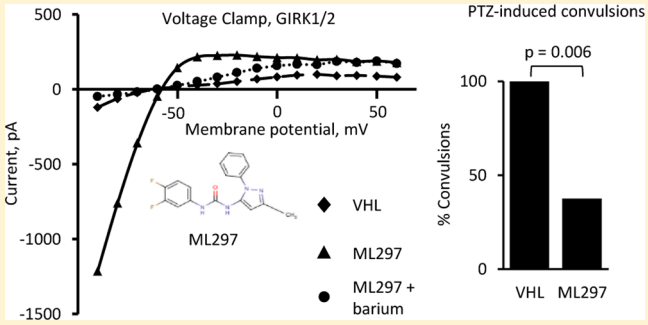

KEYWORDS: *GIRK, G-protein, inward rectifier, potassium channel, epilepsy, activator*

The G-protein activated inward rectifying potassium (K^+) channels, GIRKs, are members of a larger family of inward-rectifying potassium channels, K_{ir}s. As the name suggests, GIRK channels can be activated by pertussis toxin-sensitive G-protein-coupled receptors of the G_i subtype through interactions with the G-protein's β/γ subunits.[1−3] However, GIRK regulation is complex and both positive and negative modulation has been observed through G_s and G_q GPCRs as well as via other indirect mechanisms. GIRK regulation by GPCRs is believed to be linked to biological effects of a variety of GPCR agonists including opioids, acetylcholine, and the $GABA_B$ receptor agonist, baclofen.

The GIRK channels are comprised of four subunits, GIRK 1−4 (aka $K_{ir}3.1$−3.4),[4,5] encoded by the genes KCNJ3, KCNJ6, KCNJ9, and KCNJ5, respectively. These four subunits can form homo and heterotetramers with unique biophysical properties, regulation, and distribution (reviewed in ref 6). GIRKs are found widely expressed in the brain with the GIRK1/2 subunit combination being the most common and widespread within the cortex, hippocampus, cerebellum, and various other brain regions, while other subunit combinations, such as GIRK1/4, show very limited expression in the brain with concentrations in discrete midbrain nuclei such as the hypothalmus.[7] Although GIRK1 is widely expressed in the brain, it is not believed to form functional channels on its own.[8] However, there are GIRKs that have been reported that do not express GIRK1. These GIRKs, including homomeric GIRK2 and GIRK2/3, show restricted expression patterns in midbrain regions such as the ventral tegmental area (VTA) and substantia nigra.[9,10] Different GIRK subunit combinations also display distinct subcellular localization patterns, including pre, post, and extra-synaptic localization,[11,12] perhaps underlying a diversity of physiological roles for GIRK and GIRK regulation. GIRK expression is not limited to the brain, however. Notably, the

Received: March 5, 2013
Accepted: June 3, 2013
Published: June 3, 2013

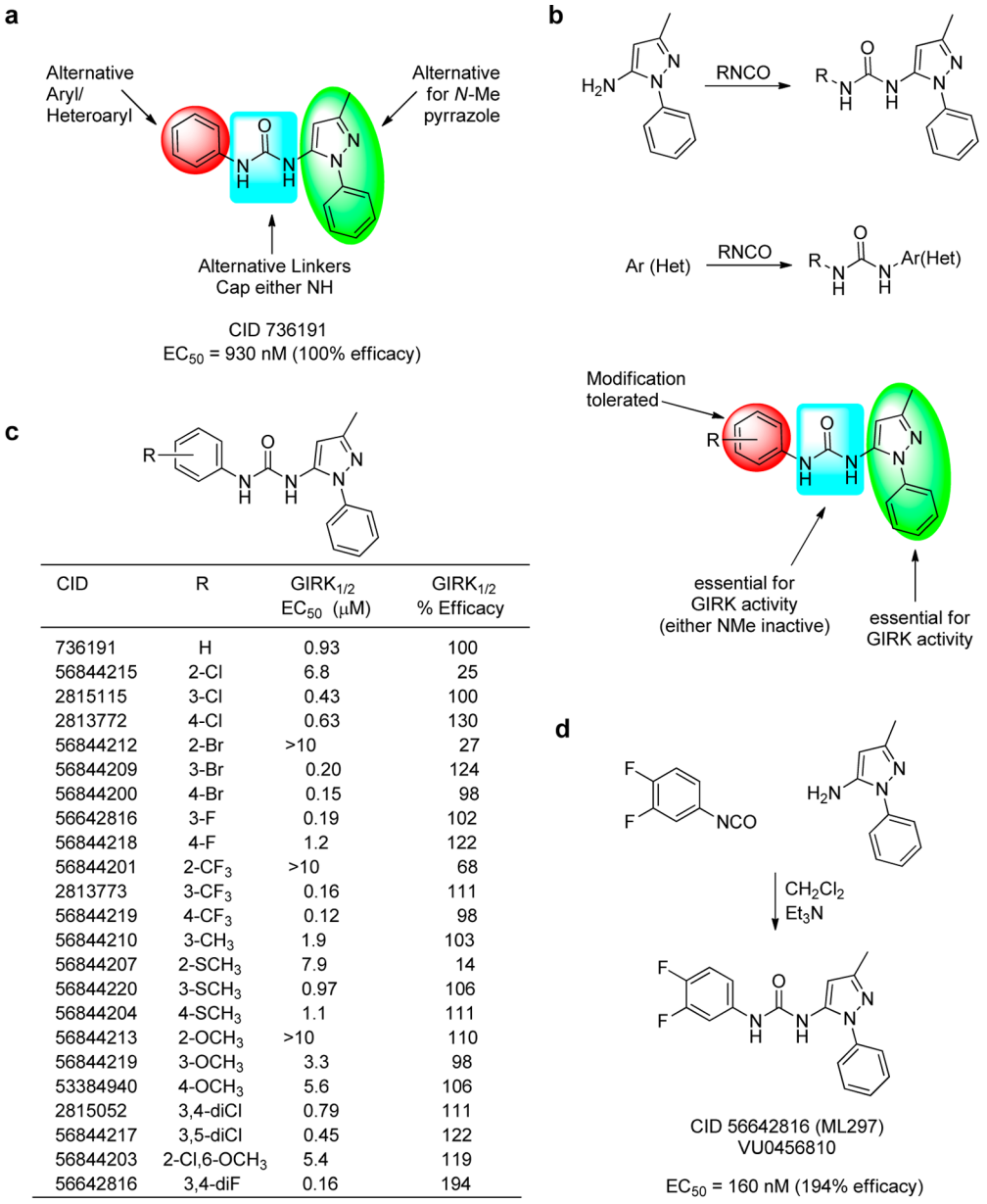

CID	R	GIRK$_{1/2}$ EC$_{50}$ (μM)	GIRK$_{1/2}$ % Efficacy
736191	H	0.93	100
56844215	2-Cl	6.8	25
2815115	3-Cl	0.43	100
2813772	4-Cl	0.63	130
56844212	2-Br	>10	27
56844209	3-Br	0.20	124
56844200	4-Br	0.15	98
56642816	3-F	0.19	102
56844218	4-F	1.2	122
56844201	2-CF_3	>10	68
2813773	3-CF_3	0.16	111
56844219	4-CF_3	0.12	98
56844210	3-CH_3	1.9	103
56844207	2-SCH_3	7.9	14
56844220	3-SCH_3	0.97	106
56844204	4-SCH_3	1.1	111
56844213	2-OCH_3	>10	110
56844219	3-OCH_3	3.3	98
53384940	4-OCH_3	5.6	106
2815052	3,4-diCl	0.79	111
56844217	3,5-diCl	0.45	122
56844203	2-Cl,6-OCH_3	5.4	119
56642816	3,4-diF	0.16	194

Figure 1. Design, synthetic strategy, and SAR leading to the discovery of the GIRK activator ML297. (a) Diversity-oriented modular design strategy to survey three regions of HTS hit CID 736191. (b) General synthetic approach for library synthesis. (c) SAR table of analogues of CID 736191. (d) Synthesis and structure of ML297 (CID 56642816, VU0456810). Potency values were obtained from triplicate determinations and the efficacy values shown are standardized to the efficacy of the parent compound in the series, CID736191, arbitrarily designated as 100%.

GIRK1/4 subunit combination is highly localized in cardiac atrial myocytes where it is responsible for the muscarinic acetylcholine activated current, I_{KAch}, involved in regulating heart rate. Because of GIRK1/4's restricted expression in atrial myocytes, it has long been thought to serve as a potential target for the treatment of atrial fibrillation.

A number of studies using subunit-specific GIRK knockout mice have produced a wide variety of interesting phenotypes that suggest roles for GIRKs in a variety of important physiological processes as well as pointing to GIRK as a target for therapeutic intervention, reviewed in ref 6. Among these are effects on addiction and withdrawal behaviors, pain perception, anxiety, spatial learning/memory, and predisposition toward seizure activity. In addition to these GIRK knockout phenotypes, emerging human genetic evidence is accumulating that may further implicate GIRK in human disease. Recent studies link GIRK1 to schizophrenia susceptibility in a Chinese population;[13] in this study, lower GIRK1 expression levels in post-mortem brains from schizophrenic and bipolar individuals were observed. Other studies have suggested GIRK2 and GIRK3's involvement in responsiveness to analgesics,[14,15] GIRK2's potential link to alcoholism,[16] as well as links between GIRK4 and early onset atrial fibrillation[17] and hyperaldosteronism.[18]

Although GIRKs have long been the focus of basic research efforts providing mounting evidence to linkages to human disease, there are very few pharmacological tools that have been reported[19] that might allow a better understanding of the roles of GIRKs in normal and pathophysiological conditions. This lack of tools has also limited our understanding of GIRKs' potential as targets for therapeutic intervention. In the GIRK inhibitor class, the compound NTC-801 stands as the sole

dx.doi.org/10.1021/cn400062a | ACS Chem. Neurosci. 2013, 4, 1278−1286

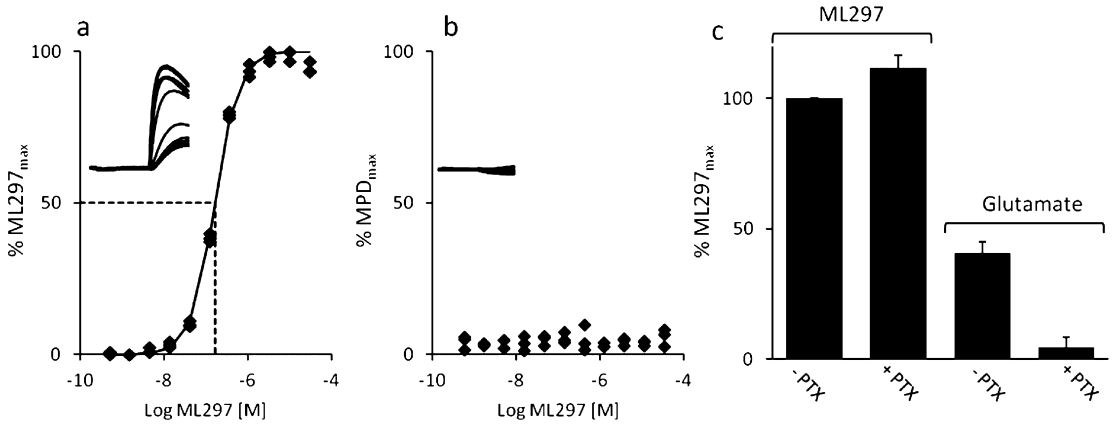

Figure 2. ML297 selectively activates GIRK1-containing GIRKs in the absence of active G_i G-proteins. Shown in (a) are thallium flux data resulting from treating GIRK1 + GIRK2 expressing cells with a ML297 concentration series. The fit shown is to triplicate data points from a representative experiment. The inset shows the raw traces from which fits were derived. Data are normalized to a maximally effective concentration of ML297. Shown in (b) are data obtained and plotted as in (a) for cells expressing GIRK2 alone. Data are normalized to a 78 mM concentration of the nonselective GIRK activator, methyl pentandiol (MPD). Shown in (c) are thallium flux traces obtained from PTX-treated GIRK1 + GIRK2 + $mGlu_8$-expressing cells in the presence of a maximally effective concentration of ML297 (10 μM) or a maximally effective concentration of glutamate (100 μM). All data shown are representative of at least three independent experiments. The scale of the inset figures in panels (a) and (b) are identical.

example of a potent and selective GIRK compound.[20] This compound, with a slight preference for the predominant cardiac form of GIRK, GIRK1/4, is presently in clinical trials for the treatment of atrial fibrillation. In addition to GPCR-mediated activation, GIRKs are also known to be activated by alcohols, including ethanol,[21,22] which may exert some of its behavioral effects through its action on GIRK. Ethanol exerts effects on many channels, including NMDA and $GABA_A$ receptors; therefore, ethanol is not a specific GIRK activator. Two recent reports have disclosed additional compounds that activate GIRK.[23,24] In the case of the natural product, naringin, a potency of ~100 μM limits the utility of the compound to in vitro assays. In,[24] the authors report the identification of both GIRK inhibitors and activators discovered by screening a library of compounds that are structurally related to fluoxetine. In the case of these compounds, the lack of structural information and other details regarding their activity and specificity preclude any substantive conclusions regarding the use of these compounds as tools to study GIRKs in vivo or in vitro.

RESULTS AND DISCUSSION

Although the GIRK family of potassium channels has been of intense research interest for nearly two decades, selective pharmacological tools have remained elusive. In particular, the lack of selective and potent GIRK activators has prevented investigators from probing the effects of selective GIRK activation in normal and pathophysiological conditions, as well as potential adverse effects induced by GIRK activation. In the present study, we report the discovery and characterization of the first potent, selective, in-vivo-active GIRK activator, ML297, and we provide intriguing data that implicates GIRK as a novel target for the treatment of epilepsy.

Previously we reported the development of a high-throughput screening (HTS)-compatible thallium flux assay for $G_{i/o}$-coupled GPCRs using GIRK as a readout.[25] This assay technology was used to conduct an HTS in cells coexpressing metabotropic glutamate receptor 8 ($mGlu_8$) and GIRK1/2 channels with the molecular libraries small molecule repository (MLSMR) compound collection as part of the Molecular Libraries Screening Center Network (MLSCN). We reasoned that the hits from this screen likely also included direct GIRK modulators; thus, we set out to use the $mGlu_8$/GIRK HTS data set in an effort to identify novel GIRK modulators. The hits from the primary screening set were evaluated for their ability to activate GIRK irrespective of modulation by a GPCR. The thallium flux-based HTS of $mGlu_8$ using GIRK1/2 as a readout yielded ~2000 hits. These hits were tested at single concentrations in HEK-293 cells expressing either $mGlu_8$ and GIRK1/2 or $mGlu_8$ without GIRK in thallium flux assays. The hits were also tested in HEK-293 cells coexpressing $mGlu_8$ and G_{qi9} in a calcium flux assay (AIDs 623869, 623952). Compounds that were only active when tested on the cells coexpressing $mGlu_8$ and GIRK1/2 were selected for further testing. From this effort (Figure 1a), we identified CID736191 (**1**), an asymmetrical urea, as a confirmed GIRK activator of GIRK1/2 with an EC_{50} of ~1 μM. The low-micromolar potency, combined with the modular nature of the chemotype, represented an attractive starting point for chemical optimization via iterative parallel synthesis.[26] Several libraries were prepared surveying alternative substituents on the aryl ring, alternative heterocycles to replace the *N*-phenyl pyrrazole, as well as alternative linkers for the urea moiety (Figure 1b). Testing of these compounds using the thallium flux assay in cell lines expressing GIRK1/2, GIRK1/4, and GIRK2/3 (AIDS 623952, 602144, 602151, 602149, 602150) resulted in clear structure–activity relationships (SAR). The *N*-phenyl pyrazole was essential for GIRK activity, as were both NH moieties of the urea linker. Productive SAR was discovered by appending substituents to the aryl ring (highlighted in red in Figure 1). Here, 2-substituents generally led to inactive compounds, whereas 3-substituted and 3,4-disubstitiuted analogues proved to be optimal (Figure 1c). Thus, chemical optimization afforded ML297 (aka VU0456810, CID 56642816), as the first potent GIRK activator (Figure 1d).

As shown in Figure 2a, in thallium flux assays ML297 showed concentration-dependent efficacy when tested on cells expressing GIRK1/2 with a measured potency of ~160 nM. ML297 was also able to activate GIRK channels comprised of

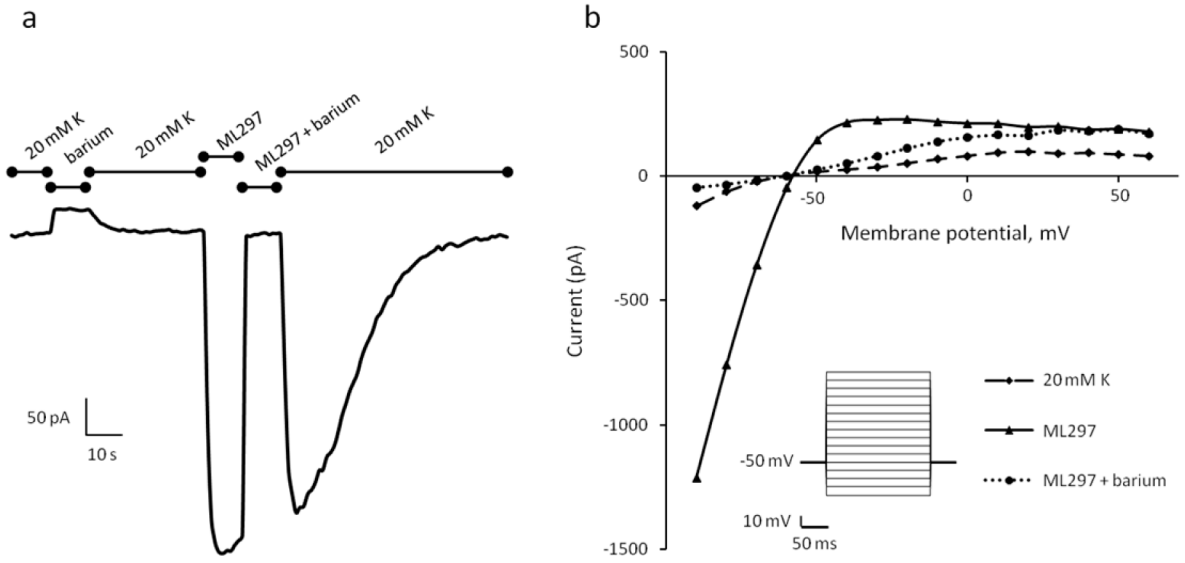

Figure 3. Electrophysiological Characterization of ML297. Shown are the results obtained from voltage-clamp experiments performed with ML297 on cells expressing GIRK1 + GIRK2. (a) Representative current traces resulting from treatment of GIRK-expressing cells, measured at a holding potential of −70 mV, with 10 μM ML297 in the presence of 20 mM extracellular K^+. The effect of ML297 is inhibited by the addition of the nonselective blocker of inward rectifying potassium channels, barium (2 mM). (b) Current−voltage relationship of currents obtained from GIRK 1 + GIRK 2-expressing cells in the presence and absence of ML297 and ML297 + barium (2 mM). All data shown represent data collected from a minimum of three experiments.

GIRK1/3 and GIRK1/4 subunit combinations (Supporting Information, Table 1a). However, ML297 showed a complete inability to modulate the activity of HEK-293 cells expressing GIRK2 alone (Figure 2b and Supporting Information, Table 1a). A similar complete lack of efficacy was observed when ML297 was tested on HEK-293 cells expressing GIRK2/3 (Supporting Information, Table 1a). Thus, it appears that ML297 is only capable of activating GIRK channels containing a GIRK1 subunit. Furthermore, none of the compounds related to ML297 that were synthesized as part of ML297's development showed any activity at non-GIRK1-containing GIRKs, regardless of their activity at GIRK1-containing channels. These observations support the hypothesis that at least a portion of the binding site for ML297 is unique to GIRK1. The fact that ML297's efficacy is limited to GIRK1-containing GIRK channels provides an excellent opportunity to begin to address questions about the roles of GIRK1 and non-GIRK1-containing GIRKs. The ability to target specific GIRK subunit combinations may also provide a basis to selectively modulate certain physiological pathways and not others, which could have important benefits when considering therapeutic uses for GIRK modulators.

To more fully investigate ML297's selectivity for GIRK1-containing GIRKs, we tested it using thallium flux assays on cells expressing the closely related potassium channel $K_{ir}2.1$ as well as two voltage-gated potassium channels, $K_v7.4$ and hERG. ML297 was inactive on $K_{ir}2.1$ and Kv7.4 and showed a partial ability (~60% at 100 μM) to inhibit the hERG potassium channel with low potency (IC_{50} ~ 10 μM, Supporting Information, Table 1b). Our selectivity studies on ML297 were further extended by submitting ML297 to the Lead Profiling (Ricerca, Concord, OH) panel of radioligand binding assays. In this panel containing 68 targets, ML297 failed to exhibit significant activity at any targets with the exception of modest activity at the $5\text{-}HT_{2b}$ receptor, the sigma σ1 receptor, and the $GABA_A$ receptor (muscimol binding site) (Supporting Information, Table 1c). Although the levels of binding (<50%) observed at the 10 μM test concentration compared to the potency of ML297 at GIRK1-containing GIRKs suggest that these other targets are not likely to be of significant concern, we wanted to rule out the possibility that $GABA_A$ receptor activation or potentiation might confound future behavioral studies. To address this possibility, we performed whole-cell voltage-clamp studies on $GABA_A$ receptors (α1, β2, γ2 subunit combination) transiently transfected in HEK-293 cells. In these studies, ML297 failed to show any activation or potentiation of GABA-evoked currents (Supporting Information, Table 1b).

In order to investigate whether ML297's activity requires the presence of an active G_i GPCR, we evaluated the effect of pertussis toxin treatment (PTX) which inactivates α_i subunits by ADP-ribosylation. As shown in Figure 2c, in HEK-293 cells coexpressing $mGlu_8$ and GIRK1/2, PTX treatment was effective at abolishing the ability of glutamate to stimulate an increase in GIRK-mediated thallium flux, while the same treatment was unable to block the effect of ML297. Thus, unlike the activation of GIRK mediated through G_i-coupled GPCRs, we found that ML297's effects were not diminished by PTX treatment. These data support the suggestion that ML297 works via direct action at the GIRK channel and does not require the presence of an activated G_i GPCR. In addition, we observed that in the cell line coexpressing $mGlu_8$ and GIRK1/2, the magnitude of thallium flux evoked by a maximally effective concentration of ML297 (10 μM) was approximately twice that evoked by a maximally effective concentration of glutamate (100 μM, Figure 2c), demonstrating that ML297 is a very effective GIRK1/2 activator. Additional studies are required to improve our understanding of the interplay between G-protein-mediated regulation of GIRK and the channel's activation by ML297 and related molecules.

To further explore the findings from thallium flux experiments, the effects of ML297 were also studied using whole-cell voltage-clamp in HEK-293 cells expressing GIRK1/2, GIRK1/4, GIRK2 and GIRK2/3. When we used standard whole-cell voltage-clamp to evaluate ML297, we found that its activity

dx.doi.org/10.1021/cn400062a | ACS Chem. Neurosci. 2013, 4, 1278−1286

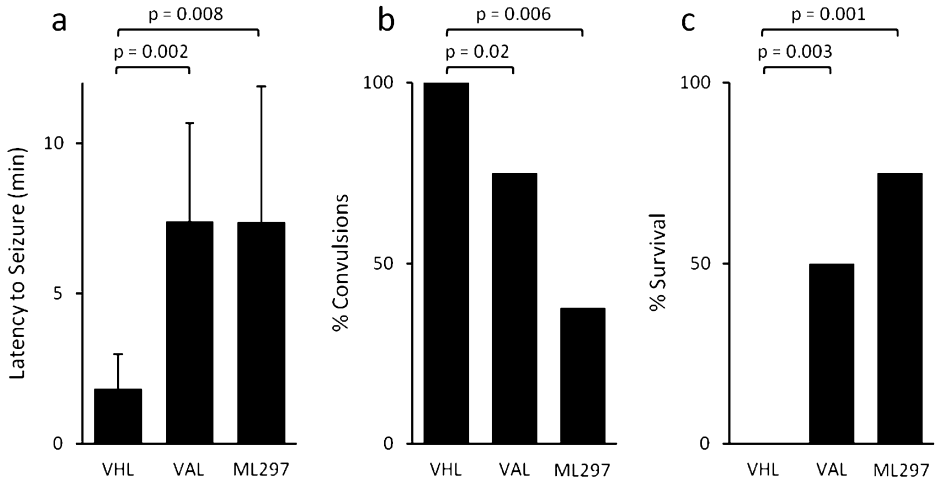

Figure 4. ML297 is active in two models of epilepsy. Shown are data obtained from mice after intraperitoneal dosing with ML297 (60 mg/kg) or sodium valproate (150 mg/kg). In (a) are the measured latencies before seizure onset in mice exposed to a lethal electrical shock. Both the antiepileptic positive control, sodium valproate (VAL), and ML297 showed highly significant delays in seizure onset. In (b) and (c) are the data obtained from mice injected with the $GABA_A$ inhibitor, PTZ. Shown in (b) are the percentage of animals tested that experienced convulsions from PTZ treatment and in (c) the percentage of animals that survived PTZ treatment. In both cases VAL and ML297 showed significant decreases in the number of animals experiencing convulsions and surviving PTZ treatment compared to vehicle (VHL)-treated controls.

profile closely matched what we observed with the thallium flux assay (Supporting Information, Table 1a) with the compound demonstrating an ability to activate GIRK1/2 and GIRK1/4 but neither GIRK2 nor GIRK2/3. Figure 3a shows inward currents evoked by the application of ML297 to GIRK1/2-expressing HEK-293 cells using a high-speed, local superfusion apparatus. The observed currents were inhibited by the well-known inhibitor of inward-rectifying potassium channels, barium. At a concentration of 2 mM (Figure 3a), barium is not fully effective at blocking all of the VU297-evoked current. However, at 10 mM barium, current levels measured are identical to those measured in the presence of either 2 or 10 mM barium in the absence of ML297 (data not shown). These data suggest the possibility that the presence of ML297 may affect barium's ability to block the channel. This possibility will be the focus of future investigations. The onset of current was rapid with 90% of maximal amplitude obtained after approximately 2 s of application. However, as illustrated in Figure 3a, when ML297 application was terminated, washout was a slower process requiring nearly a minute. The rate of ML297 washout did not appear to be affected by the presence of barium (Figure 3a) or absence of barium (data not shown). Figure 3b shows that ML297 was able to evoke inward currents that maintained the ion selectivity and inward rectification normally observed with the GIRK channel (Figure 3b). Overall, our data suggest that ML297 is highly selective for GIRK1-containing GIRK channels and thus represents the first reported potent, effective, and selective GIRK activator compound.

Following characterization of ML297's ability to potently and selectively activate GIRK in vitro, we were eager to investigate the in vivo pharmacological properties of ML297 and to explore its value as a tool for understanding a GIRK activator's potential for therapeutic benefit. Prior to conducting these studies, we performed a number of in vitro and in vivo distribution, metabolism, and pharmacokinetic assays (DMPK) to assess ML297's suitability as an in vivo tool. ML297 showed good solubility (17.5 μM), modest plasma protein binding (mouse f_u, 0.026) with high mouse liver microsome metabolism (Cl_{HEP} = 88 mL/min/kg, Supporting Information, Table 2) in vitro. When ML297 was administered by intraperitoneal injection (IP, 60 mg/kg) into mice, we observed a maximal free plasma concentration (C_{max}) of 640 nM with a corresponding free brain C_{max} of 130 nM, producing a brain-to-plasma ratio of 0.2 (Supporting Information, Table 2). A single major metabolite was identified for ML297, ML297-M1, resulting from the oxidation of the 3-methyl moiety to afford the corresponding primary alcohol (Supporting Information, Figure 1), which proved to be inactive on GIRK1/2 and GIRK1/4. These features of ML297, while suboptimal with respect to metabolic stability and relative brain penetration, were suitable for in vivo efficacy studies.

To begin to explore the potential for GIRK activators as in vivo tools and potential therapeutic targets, we chose to investigate the effects of systemic administration of ML297. First, we performed an ascending dose study (10, 30, 60 mg/kg, intraperitoneal injection) in mice. At all doses tested, the animals appeared normal and not under obvious distress. We went on to more thoroughly examined ML297's effects on locomotor activity as well as effects on motor function and coordination. As a general test of locomotor activity, we assessed the activity of ML297 (60 mg/kg) and vehicle treated animals in their home cage using the SmartCage system[27] immediately following injection. In the ML297-treated animals, we noted an immediate decrease in locomotor activity compared to the control group (Supporting Information, Figure 2a). As a test of ML297's effects on motor function and coordination, mice treated with a 60 mg/kg dose of ML297 were examined using a rotarod apparatus. When compared to the vehicle-treated animals, the ML297-treated group showed a modest (14%) but insignificant (p = 0.7) decrease in performance on the rotarod (Supporting Information, Figure 2b). Thus, ML297's effects on generalized locomotor activity do not appear to be through compound-induced motor deficits but instead may be mediated through sedation. Future studies will focus on increasing our understanding of the mechanism by which ML297 produces the observed decreases in locomotion.

Since previous development of GIRK2 knockout animals has revealed an epilepsy phenotype, suggesting a role for GIRK in regulating excitability,[28] and because the GIRK1/2 subunit combination is most prevalent in the brain, we reasoned that a GIRK1/2 activator might produce effects in an epilepsy model in vivo. Therefore, we evaluated ML297 in a maximal electroshock (MES) model of epilepsy in mice. At the 60 mg/kg dose we observed a robust increase in the latency of seizure onset equivalent to that observed with a 150 mg/kg dose of the known antiepileptic, sodium valproate (Figure 4a). Both the effects of ML297 and sodium valproate were highly significant compared to vehicle-treated animals with measured p-values of 0.008 and 0.002, respectively (n = 7, 8, 10, and 10 animals for ML297, sodium valproate, and vehicle control, respectively). Upon achieving activity in the MES model, we investigated the efficacy of ML297 in a chemically induced epilepsy model. In this model, the $GABA_A$ antagonist pentylenetetrazol (PTZ) was administered to induce seizures after administration of ML297 (60 mg/kg), sodium valproate (150 mg/kg), or vehicle. As in the MES model, both sodium valproate and ML297 were effective when compared to the vehicle control (Figure 4 b,c). ML297 showed a highly significant ability to both prevent convulsions (p = 0.006) and prevent fatality of the PTZ treatment (p = 0.001) with most of the animals treated with ML297 experiencing neither convulsions nor death. Five out of eight ML297-treated animals did not experience convulsions compared to eight out of eight animals experiencing convulsions in the control group. Six out of eight ML297-treated animals survived PTZ treatment compared to eight out of eight animals that died in the control group within the 20 min time frame of the testing procedure.

Taken together, our data provide the first demonstration of the discovery, improvement, and characterization of a potent, selective, in vivo-active GIRK activator, paving the way for a more complete understanding of GIRKs' role in physiology as well as the exploration of its potential for a wide range of therapeutic indications. Our data also point to key structural differences in GIRK1 and non-GIRK1 containing GIRKs, which may lead to new insights into GIRK structure, function, and regulation. While ML297 shows exquisite selectivity when considering GIRK1 vs non-GIRK1-containing GIRKs, it only shows a modest preference for the activation of the GIRK1/2 subunit combination versus GIRK1/3 or GIRK1/4, with measured potencies all within a 6-fold range. SAR developed thus far in the ML297 scaffold suggests a pathway forward in this chemotype to improve both GIRK1/2 selectivity and DMPK properties. Ongoing medicinal chemistry efforts will focus on development of improved probes. Despite the fact that ML297's DMPK properties were suboptimal with a relatively short half-life, modest free-fraction, and modest brain penetration, we observed robust activity in two epilepsy models. Regardless of whether epilepsy was initiated chemically with PTZ or via electroshock, ML297 showed equal or greater efficacy compared to a clinically active antiseizure medication, sodium valproate. These data support a role for selective GIRK activation in controlling excitability and provide the first evidence for the exciting possibility that GIRK may, in fact, represent an attractive new target for antiepileptic drugs. ML297 and other more selective probes with improved DMPK properties will provide a basis to begin to probe GIRK1-containing GIRKs roles and therapeutic potential in a variety of other indications including anxiety, pain, feeding, and addiction/withdrawal.

METHODS

Compound Synthesis. All reagents were purchased from Sigma-Aldrich Corp., TCI America, and Rieke Metals, Inc. and were used without purification. All polymer supported reagents were purchased from Biotage, Inc. Analytical thin-layer chromatography (TLC) was performed on 250 μm silica gel plates from Sorbent Technologies. Visualization was accomplished via UV light, and/or the use of ninhydrin and potassium permanganate solutions followed by application of heat. Chromatography was performed using Silica Gel 60 (230−400 mesh) from Sorbent Technologies or Silica RediSep Rf flash columns on a CombiFlash Rf automated flash chromatography system. All ^{1}H, ^{13}C and ^{19}F NMR spectra were recorded on a Bruker AV-400 (400 MHz) instrument. Chemical shifts are reported in ppm relative to residual solvent peaks as an internal standard set to δ 7.26 and δ 77.16 ($CDCl_3$). Data are reported as follows: chemical shift, multiplicity (s = singlet, d = doublet, t = triplet, q = quartet, p = pentet br = broad, dd = doublet of doublets, dq = doublet of quartets, td = triplet of doublets, pd = pentet of doublets, m = multiplet), coupling constant (Hz), integration. Low resolution mass spectra (LCMS) were obtained on an Agilent 1200 LCMS with electrospray ionization. High resolution mass spectra (HRMS) were recorded on a Waters Qtof-API-US plus Acquity system with ES as the ion source. Analytical high pressure liquid chromatography (HPLC) was performed on an Agilent 1200 analytical LCMS with UV detection at 214 and 254 nm along with ELSD detection.

1-(3,4-Difluorophenyl)-3-(3-methyl-1-phenyl-1*H*-pyrazol-5-yl)urea (ML297). To a solution of 3-methyl-1-phenyl-1*H*-pyrazol-5-amine (500 mg,2.9 mmol) in 11.5 mL of CH_2Cl_2 was added 3,4-difluorophenylisocyanate (0.68 mL, 5.8 mmol). After 16 h, the reaction was concentrated and the residue was purified by column chromatography with MeOH/CH_2Cl_2 to afford 418 mg (65%) of the desired product. ^{1}H NMR (MeOD) δ 7.50 (m, 6H), 7.13 (dd, J = 19.2, 9.6 Hz, 1H), 6.98 (m, 1H), 6.35 (s, 1H), 2.27 (s, 3H); ^{13}C NMR (MeOD) δ 152.3, 149.8 (dd, J = 13.2, 242.9 Hz), 149.1, 145.8 (dd, J = 12.8, 240.4 Hz), 137.7 (d, 13.1 Hz), 135.6 (dd, J = 2.9, 9.0 Hz), 129.2, 128.1, 125.0, 116.7 (d, J = 18.1), 114.5 (dd, 3.6, 5.7 Hz), 107.9 (d, J = 21.8 Hz), 98.4, 12.2; ^{19}F NMR (MeOD) δ −137.3 (d, J = 22.6 Hz), −145.9 (d, J = 22.6 Hz); HRMS calculated for $C_{17}H_{14}F_2N_4O$ (M+H)+ m/z: 329.1214, measured 329.1211 m/z.

Cell Line Construction and Cell Culture. HEK-293 cells coexpressing human GIRK1/2 and rat $mGlu_8$ were generated as previously described.[25] A HEK-293 cell line (ATCC, Manassas, VA) expressing human GIRK1 and human GIRK2 was constructed by transfecting HEK-293 cells with GIRK1 and GIRK2 (Origene, Rockville, MD) cloned into the pBudCE4.1 vector (Life Technologies, Carlsbad, CA) using FuGene 6 (Promega, Madison, WI) transfection reagent. Unless otherwise noted, other ion channel-expressing cells were prepared by transfecting HEK-293 cells with individual or combinations of subunits: GIRK1, pCMV6-A-BSD; GIRK2, pCMV6-A-puro; GIRK3, pCMV6-A-hygro; GIRK 4, pCMV6-A-AC; Kv7.4, pIRESneo3. The K_{ir}2.1 and hERG-expressing cell lines were made by transfecting T-REx-293 cells (Life Technologies, Carlsbad, CA) with K_{ir}2.1 and Kv11.1, respectively, cloned into pcDNA5TO. Monoclonal cell lines were produced by limiting-dilution cloning of antibiotic-resistant cells and functional selection using the thallium flux assay described below. Unless otherwise noted, cells were maintained in Minimal Essential Medium, Alpha Medium (Mediatech, Manassas, VA) supplemented with 10% fetal bovine serum (Sigma-Aldrich, Saint Louis, MO), and GlutaGro (Mediatech, Manassas, VA), referred to henceforth as cell culture medium. Cell culture medium was further supplemented with selection antibiotics, as appropriate.

Thallium Flux Assays. For thallium flux assays, cells were dislodged from tissue culture flasks using TrypLE Express (Life Technologies, Carlsbad, CA), transferred to a 50 mL centrifuge tube, and spun at 500g for 2 min. The supernatant solution was removed by aspiration and the pellet was resuspended at concentration of ∼1000 cells/μL. Twenty μL/well of the cell suspension was transferred to 384-well, amine-coated assay plates (cat# 354719, BD, Franklin Lakes, NJ) using an electronic multichannel pipet. Plated cells were incubated

overnight in a humidified 5% CO_2 cell culture incubator at 37 °C. After overnight incubation the cell culture medium was replaced with 20 μL/well of a dye loading solution containing assay buffer (Hanks Balanced Salt Solution plus 20 mM HEPES, pH 7.3), 0.04% (w/v) Pluronic F-127 (Sigma-Aldrich, St. Louis, MO), and 1.2 μM of the thallium-sensitive dye Thallos-AM (TEFlabs, Austin, TX). Following a 1 h incubation at room temperature, the dye loading solution was replaced with 20 μL/well assay buffer and the plates were loaded into a Hamamatsu FDSS 6000 (Bridgewater, NJ). Data were acquired at 1 Hz (excitation 470 ± 20 nm, emission 540 ± 30 nm) for ten seconds, followed by the addition of 20 μL/well of test compounds (prepared as described below), followed by an additional 4 min of data collection. At the 4 min mark, 10 μL/well of a thallium stimulus buffer was added and data collection continued for an additional 2 min. The thallium stimulus buffer contained (in mM) 125 $NaHCO_3$, 1.8 $CaSO_4$, 1 $MgSO_4$, 5 glucose, 2.4 Tl_2SO_4, 10 mM HEPES pH 7.4. For the thallium flux assay of the GIRK1 + GIRK3 containing cell line, the Tl_2SO_4 concentration in the stimulus buffer was 12 mM. For the thallium flux assays of hERG a modified assay buffer was used for test compound dilution where 60 mM of the NaCl was replaced with 60 mM KCl (High-K^+ assay buffer). Additionally, for the hERG assay, the time of incubation with compound prior to thallium stimulus buffer addition was 20 min. For experiments with PTX, cells expressing GIRK1 + GIRK2 + $mGlu_8$ were plated and incubated overnight in a humidified 5% CO_2 cell culture incubator at 37 °C. On the next day the cell culture medium was replaced with 20 μL/well cell culture medium containing 600 ng/mL PTX (Tocris, Bristol, UK). Plates containing PTX were returned to the cell culture incubator for 8 h after which time the cell culture medium was removed and the assays conducted as described above for other thallium flux assays with the addition of varying concentrations of glutamate to the thallium stimulus buffer for the activation of the $mGlu_8$ receptor coexpressed with GIRK1 + GIRK2.

Compounds were dissolved in DMSO to a concentration of 10–100 mM. Fourty-five microliter aliquots were placed in 384-well, flat-bottom, Echo-qualified, polypropylene plates (Labcyte, Sunnyvale, CA). Samples were diluted in 3-fold steps in DMSO using a Bravo liquid handler (Agilent, Santa Clara, CA) with tip changes between each dilution step. Serially diluted samples were transferred to 384-well, round-bottom, polypropylene plates (Greiner, Monroe, NC) using an Echo555 plate reformatter (Labcyte, Sunnyvale, CA). Samples were then diluted with assay buffer using a Combi (Thermo Fisher, Waltham, MA) and mixed vigorously using a Teleshake (Inheco, Martinsried, Germany). Diluted samples were used within an hour of dilution. Final DMSO concentrations in all studies were 0.3% or less.

Thallium flux data were analyzed using the method described in ref 25 in Excel (Microsoft, Redmond, WA) by first dividing each point in each wave by the first point in that wave (F/F_0) and then subtracting the average of the vehicle control waves from each wave. The slopes of these vehicle control-subtracted waves we calculated from ten data points beginning 2 s after thallium stimulus addition. The choice to use slope values instead of amplitudes helps prevent shifts in potency that can result from indicator dye or detector saturation due to large increases in channel activity. Slope values were used to obtain fits to a four parameter logistic equation in XLfit (IDBS, Guildford, Surrey, UK).

Electrophysiology. For whole-cell, voltage-clamp assays, compound were diluted from DMSO stocks into 20 mM KCl, 140 mM NaCl, 0.5 mM $CaCl_2$, 2 mM $MgCl_2$ and 10 mM HEPES (pH 7.4), referred to hereafter as 20K extracellular solution. The GIRK activator probe, ML297, was serially diluted in DMSO manually from a 100 mM DMSO stock further diluted to make test samples in 20K extracellular solution.

A single-cell suspension of HEK-293 cells stably transfected with the appropriate ion channels was plated into TC-treated 35 mm polystyrene dishes at ∼15% confluence and incubated overnight in a 5% CO_2 cell culture incubator at 37 °C. Whole-cell patch-clamp recordings were performed 24–72 h after plating. Borosilicate glass electrodes (5–7 mΩ resistance) were filled with intracellular solution (130 mM KCl, 20 mM NaCl, 5 mM EGTA, 5.46 mM $MgCl_2$, and 10 mM HEPES, pH 7.4). Whole-cell currents were recorded in 20K extracellular solution at −70 mV using a Pico1 amplifier (Tecella, Foothill Ranch, CA) controlled by WINWCP 4.X (University of Strathclyde, Glasgow, Scotland, UK). Signals were compensated for electrode capacitance, cellular capacitance and series resistance. Signals were filtered at 1 kHz, and digitized at 5 kHz. Solutions were applied to cells with a Valvelink 8.2 (Automate Scientific, Berkeley, CA) rapid, valve-controlled perfusion system with an in-house-made local superfusion manifold. Barium-sensitive current measurements were obtained by applying the nonselective K_{ir} inhibitor, 2 mM $BaCl_2$, in 20K extracellular solution in the absence and presence of test compounds and measuring the amplitude of the barium-sensitive current. For testing activity of ML297 on $GABA_A$ receptors, HEK-293 cells were transiently transfected with $GABA_A$ subunits α1, β2, γ2 using Fugene 6 (Promega, Madison, WI). One day after transfection, cells were plate into 35 mm polystyrene dishes, incubated and recorded as described above. For $GABA_A$ receptor potentiation studies, ML297 was added in the presence of 3 μM GABA.

Voltage-clamp data were analyzed by converting current amplitudes to current density by dividing by each cell's membrane capacitance estimated from capacitance compensation. For concentration–response experiments, barium-sensitive, steady-state current density values obtained at different compound concentrations were fit using a four-parameter logistic equation in XLfit.

DMPK Methods. In vitro metabolism of ML297 was investigated in mouse hepatic microsomes (BD Biosciences, San Jose, CA) using substrate depletion methodology (% test compound remaining). Hepatic microsomes (0.5 mg/mL) and 1 μM test compound were incubated in 100 mM potassium phosphate pH 7.4 buffer with 3 mM $MgCl_2$ at 37 °C with constant shaking. After a 5 min preincubation, the reaction was initiated by addition of NADPH (1 mM). At selected time intervals (0, 3, 7, 15, 25, and 45 min), 50 μL aliquots were taken and subsequently placed into a 96-well plate containing 150 μL of cold acetonitrile with internal standard (50 ng/mL carbamazepine). Plates were then centrifuged at 3000 rcf (4 °C) for 10 min, and the supernatant solution was transferred to a separate 96-well plate and diluted 1:1 with water for LC/MS/MS analysis. The in vitro half-life ($T_{1/2}$, min, eq 1), intrinsic clearance (CL_{int}, mL/min/kg, eq 2) and subsequent predicted hepatic clearance (CL_{hep}, mL/min/kg, eq 3) were determined employing the following equations:

$$T_{1/2} = \frac{\ln(2)}{k} \tag{1}$$

where k represents the slope from linear regression analysis of the natural log percent remaining of test compound as a function of incubation time

$$\mathrm{CL_{int}} = \frac{0.693}{\text{in vitro } T_{1/2}} \times \frac{\text{mL incubation}}{\text{mg microsomes}} \times \frac{45 \text{ mg microsomes}}{\text{g liver}} \times \frac{20^a \text{ g liver}}{\text{kg body weight}} \tag{2}$$

where the superscript "a" represents scale-up factor: 87.5 (mouse), and

$$\mathrm{CL_{hep}} = \frac{Q_h \times CL_{int}}{Q_h + CL_{int}} \tag{3}$$

where Q_h (hepatic blood flow, mL/min/kg) is 90 (mouse).

Plasma protein binding of ML297 was determined in plasma via equilibrium dialysis employing single-use RED Plates with inserts (ThermoFisher, Waltham, MA). Briefly plasma (220 μL) was added to a 96-well plate containing test compound (5 μL) and mixed thoroughly. Subsequently, 200 μL of the plasma-test compound mixture was transferred to the *cis* chamber of the RED plate, with an accompanying 350 μL of phosphate buffer (25 mM, pH 7.4) in the *trans* chamber. The RED plate was sealed and incubated 4 h at 37 °C with shaking. At completion, 50 μL aliquots from each chamber were diluted 1:1 (50 μL) with either plasma (*cis*) or buffer (*trans*) and transferred to a new 96-well plate, at which time ice-cold acetonitrile

(2 volumes) was added. The plate was centrifuged (3000 rcf, 10 min) and supernatant solutions transferred to a new 96-well plate. The sealed plate was stored at −20 °C until LC/MS/MS analysis.

Liquid Chromatography/Mass Spectrometry Analysis for in Vitro Experiments. ML297 was analyzed on a ThermoFisher TSQ Quantum Ultra triple quadrupole mass spectrometer via electrospray ionization (ESI) with two ThemoFisher Accella pumps (San Jose, CA), and a CTC PAL autosampler (Leap Technologies, Carrboro, NC). Analytes were separated by gradient elution using a Thermo-Fisher Hypersil Gold (2.1 × 30 mm, 1.9 μm) column at 40 °C. HPLC mobile phase A was 0.1% formic acid in water and mobile phase B was 0.1% formic acid in acetonitrile. The gradient started at 10% B after a 0.2 min hold and was linearly increased to 95% B over 0.8 min; hold at 95% B for 0.2 min; returned to 10% B in 0.1 min. The total run time was 1.3 min and the HPLC flow rate was 0.8 mL/min. Compound optimization, data collection and processing were performed using Thermo Electron's QuickQuan software (v2.3) and Xcalibur (v2.0.7 SP1).

In Vivo Pharmacokinetic Study. Compound(s) were formulated in 10% Tween80 in sterile water at the concentration of 3.33 mg/mL and administered IP to male C57 BL6 mice weighing 20 to 25 g (Harlan, Indianapolis, IN) at the dose of 60 mg/kg. The blood (cardiac puncture) and brain were collected at 30 min after dosing. Animals were euthanized and decapitated, and the brains were removed, thoroughly washed in cold phosphate-buffered saline, and immediately frozen on dry ice. Plasma was separated by centrifugation (4000 rcf, 4 °C) and stored at −80 °C until analysis. On the day of analysis, frozen whole-rat brains were weighed and added to 1:3 (w/w) parts of 70:30 isopropanol:water. The mixture was then subjected to mechanical homogenation employing a Mini-Beadbeater and 1.0 mm Zirconia/Silica Beads (BioSpec Products, Bartlesville, OK) followed by centrifugation. The sample extraction of plasma (20 μL) or brain homogenate (20 μL) was performed using three volumes of ice-cold acetonitrile containing an internal standard (50 ng/mL carbamazepine). The samples were centrifuged (3000 rcf, 5 min) and supernatant solutions were transferred and diluted 1:1 (supernatant: water) into a new 96-well plate, which was then sealed in preparation for LC/MS/MS analysis.

LC/MS/MS Bioanalysis of Samples from in Vivo Studies. In vivo samples were analyzed via electrospray ionization (ESI) on a QTrap 5500 (AB Sciex, Foster City, CA) triple-quadrupole linear ion trap instrument that was coupled with LC-20AD pumps (Shimadzu, Columbia, MD) and a Leap Technologies CTC PAL autosampler. Analytes were separated by gradient elution using a Fortis C18 2.1 × 50 mm, 3 μm column (Fortis Technologies Ltd., Cheshire, UK) at 40 °C. HPLC mobile phase A was 0.1% formic acid in water (pH unadjusted), mobile phase B was 0.1% formic acid in acetonitrile (pH unadjusted). The gradient started at 30% B after a 0.2 min hold and was linearly increased to 95% B over 0.6 min; held at 90% B for 0.7 min and returned to 10% B in 0.1 min followed by a re-equilibration (0.9 min). The total run time was 2.5 min and the HPLC flow rate was 0.5 mL/min. The source temperature was set at 500 °C and mass spectral analyses were performed using multiple reaction monitoring (MRM), with transitions specific for each compound utilizing a AbSciex Turbo-Ionspray source in positive ionization mode (5.0 kV spray voltage). The calibration curves were constructed, and linear response was obtained in the range of 0.5 to 5,000 ng/mL, by adding known amounts of VU0465810 in blank brain homogenate or plasma. All data were analyzed using AB Sciex Analyst software v1.5.1. The final PK parameters were calculated by noncompartmental analysis using Phoenix (version 6.2) (Pharsight Inc., Mountain View, CA).

In Vivo Pharmacology Assays. For the PTZ-induced seizure model, male mice (C57/BL6, 8−10 months old, approximately 30 g) were injected intraperitoneally with either ML297 (60 mg/kg), sodium valproate (150 mg/kg), or vehicle (2% DMSO in 0.5% aqueous hydroxypropyl cellulose). After 30 min, PTZ was administered intraperitoneally (40 mg/kg). Immediately following administration of PTZ, the amount of time elapsed until the onset of convulsions, and death was recorded. If a mouse did not die after 20 min post-PTZ, the mouse was euthanized by isoflurane inhalation. The average convulsion latencies (in minutes) and the fatality rates of the ML297 group, the sodium valproate group, and the vehicle group were compared (n = 8 mice/group).

For the maximal electroshock seizure (MES) model, male, C57/BL6 mice (8−10 months old, approximately 30 g), were injected intraperitoneally with either ML297 (60 mg/kg), sodium valproate (150 mg/kg) or vehicle. MES stimulation was applied, 30 min after injection, through transauricular (ear-clip) electrodes from an electroshock apparatus, HSE Shock Stimulator Type 221, (Harvard Apparatus, Holliston, MA) using the following parameters: 100 mA fixed current, a 50−60 Hz pulse frequency, a 0.6 ms pulse width, and a 0.3 s stimulus duration. Animals were restrained by hand when applying the electrodes and released at the moment of stimulation to permit observation of the seizure throughout its entire course. Upon completion of the electrical stimulus, the time to onset of seizures was recorded. A 10 min cutoff was applied to all mice after which time the mice were euthanized by isoflurane inhalation. In this modified MES test, the electrical stimulus that was applied was sufficient to induce seizures and death from maximal seizure in 100% of the mice. For the MES study, the test groups contained 10 animals, 8 animals, and 7 animals for the vehicle, sodium valproate, and ML297 treatments, respectively.

In all cases, experiments were conducted in a blind manner with respect to the experimenters. Data were evaluated in Excel using one-tailed, unpaired Student's t test, assuming populations with unequal variance.

■ ASSOCIATED CONTENT

Ⓢ Supporting Information

Comparisons of potencies of ML297 on different GIRK subunit combinations, results of selectivity testing for ML297 conducted by Ricerca, a summary of murine in vitro and in vivo DMPK data for ML297, measures of locomotor activity of mice treated with ML297, and performance of ML297 treated mice in rotarod tesing. This material is available free of charge via the Internet at http://pubs.acs.org.

■ AUTHOR INFORMATION

Corresponding Author

*Mailing address: Department of Pharmacology, Vanderbilt University School of Medicine, 824 Preston Research Building, Nashville, TN 37232.

Author Contributions

C.D.W. conceived and designed the overall study. E.D., K.K., Y.D., and C.D.W. performed the thallium flux experiments. K.K. performed the electrophysiology experiments. I.R., G.S., and C.W.L. designed the chemical synthesis. I.R. performed the chemical synthesis. J.S.D. designed the DMPK studies. R.D.M. performed the DMPK studies. X.X. designed the pharmacodynamic studies. C.P., A.M., L.Y., and B.Z. performed the pharmacodynamic studies. All authors contributed to experimental analysis and commented on the manuscript. C.D.W., C.W.L., and X.X. cowrote the manuscript. K.K. and I.R. equally contributed to this manuscript.

Funding

MH074427 to C.D.W., MH084659 to C.W.L., MH076398 to C.M.N., and R01MH078194 to X.X. ML297 is an MLPCN probe, denoted ML297, and is freely available upon request.

Notes

The authors declare the following competing financial interest(s): X. Xie is the founder and a stockholder of AfaSci, Inc. C. Weaver is the inventor of Thallos dye used in the thallium flux experiments that is sold by TEFlabs under a license from Vanderbilt University. All other coauthors declare no competing financial interests.

■ ACKNOWLEDGMENTS

The authors acknowledge the contributions of the Vanderbilt Institute of Chemical Biology's High-throughput Screening and Chemical Synthesis Cores as well as the Vanderbilt MLSCN Screening Center and MLPCN Specialize Chemistry Center.

■ REFERENCES

(1) Logothetis, D. E., Kurachi, Y., Galper, J., Neer, E. J., and Clapham, D. E. (1987) The beta gamma subunits of GTP-binding proteins activate the muscarinic K+ channel in heart. *Nature 325*, 321−326.

(2) Wickman, K. D., Iñiguez-Lluhl, J. A., Davenport, P. A., Taussig, R., Krapivinsky, G. B., Linder, M. E., Gilman, A. G., and Clapham, D. E. (1994) Recombinant G-protein beta gamma-subunits activate the muscarinic-gated atrial potassium channel. *Nature 368*, 255−257.

(3) Reuveny, E., Slesinger, P. A., Inglese, J., Morales, J. M., Iñiguez-Lluhi, J. A., Lefkowitz, R. J., Bourne, H. R., Jan, Y. N., and Jan, L. Y. (1994) Activation of the cloned muscarinic potassium channel by G protein beta gamma subunits. *Nature 370*, 143−146.

(4) Lesage, F., Duprat, F., Fink, M., Guillemare, E., Coppola, T., Lazdunski, M., and Hugnot, J. P. (1994) Cloning provides evidence for a family of inward rectifier and G-protein coupled K+ channels in the brain. *FEBS Lett. 353*, 37−42.

(5) Krapivinsky, G., Gordon, E. A., Wickman, K., Velimirović, B., Krapivinsky, L., and Clapham, D. E. (1995) The G-protein-gated atrial K+ channel IKACh is a heteromultimer of two inwardly rectifying K(+)-channel proteins. *Nature 374*, 135−141.

(6) Luscher, C., and Slesinger, P. (2010) Emerging roles for G protein-gated inwardly rectifying potassium (GIRK) channels in health and disease. *Nat. Rev. Neurosci. 11*, 301−315.

(7) Kloukina, V., Herzer, S., Karlsson, N., Perez, M., Daraio, T., and Meister, B. (2012) G-protein-gated inwardly rectifying K+ channel 4 (GIRK4) immunoreactivity in chemically defined neurons of the hypothalamic arcuate nucleus that control body weight. *J. Chem. Neuroanat. 44*, 14−23.

(8) Hedin, K. E., Lim, N. F., and Clapham, D. E. (1996) Cloning of a Xenopus laevis inwardly rectifying K+ channel subunit that permits GIRK1 expression of IKACh currents in oocytes. *Neuron 16*, 423−429.

(9) Inanobe, A., Yoshimoto, Y., Horio, Y., Morishige, K. I., Hibino, H., Matsumoto, S., Tokunaga, Y., Maeda, T., Hata, Y., Takai, Y., and Kurachi, Y. (1999) Characterization of G-protein-gated K+ channels composed of Kir3.2 subunits in dopaminergic neurons of the substantia nigra. *J. Neurosci. 19*, 1006−1017.

(10) Cruz, H. G., Ivanova, T., Lunn, M. L., Stoffel, M., Slesinger, P. A., and Lüscher, C. (2004) Bi-directional effects of GABA(B) receptor agonists on the mesolimbic dopamine system. *Nat. Neurosci. 7*, 153−159.

(11) Fernández-Alacid, L., Aguado, C., Ciruela, F., Martín, R., Colón, J., Cabañero, M. J., Gassmann, M., Watanabe, M., Shigemoto, R., Wickman, K., Bettler, B., Sánchez-Prieto, J., and Luján, R. (2009) Subcellular compartment-specific molecular diversity of pre- and post-synaptic GABA-activated GIRK channels in Purkinje cells. *J. Neurochem. 110*, 1363−1376.

(12) Lujan, R., Maylie, J., and Adelman, J. (2009) New sites of action for GIRK and SK channels. *Nat. Rev. Neurosci. 10*, 475−480.

(13) Yamada, K., Iwayama, Y., Toyota, T., Ohnishi, T., Ohba, H., Maekawa, M., and Yoshikawa, T. (2012) Association study of the KCNJ3 gene as a susceptibility candidate for schizophrenia in the Chinese population. *Hum. Genet. 131*, 443−451.

(14) Nishizawa, D., Nagashima, M., Katoh, R., Satoh, Y., Tagami, M., Kasai, S., Ogai, Y., Han, W., Hasegawa, J., Shimoyama, N., Sora, I., Hayashida, M., and Ikeda, K. (2009) Association between KCNJ6 (GIRK2) gene polymorphisms and postoperative analgesic requirements after major abdominal surgery. *PLoS One 4*, e7060.

(15) Smith, S. B., Marker, C. L., Perry, C., Liao, G., Sotocinal, S. G., Austin, J. S., Melmed, K., Clark, J. D., Peltz, G., Wickman, K., and Mogil, J. S. (2008) Quantitative trait locus and computational mapping identifies Kcnj9 (GIRK3) as a candidate gene affecting analgesia from multiple drug classes. *Pharmacogenet. Genomics 18*, 231−241.

(16) Kang, S. J., Rangaswamy, M., Manz, N., Wang, J. C., Wetherill, L., Hinrichs, T., Almasy, L., Brooks, A., Chorlian, D. B., Dick, D., Hesselbrock, V., Kramer, J., Kuperman, S., Nurnberger, J., Jr., Rice, J., Schuckit, M., Tischfield, J., Bierut, L. J., Edenberg, H. J., Goate, A., Foroud, T., and Porjesz, B. (2012) Family-based genome-wide association study of frontal theta oscillations identifies potassium channel gene KCNJ6. *Genes, Brain Behav. 11*, 712−719.

(17) Jabbari, J., Olesen, M. S., Holst, A. G., Nielsen, J. B., Haunso, S., and Svendsen, J. H. (2011) Common polymorphisms in KCNJ5 are associated with early-onset lone atrial fibrillation in Caucasians. *Cardiology 118*, 116−120.

(18) Zennaro, M. C., and Jeunemaitre, X. (2011) Mutations in KCNJ5 gene cause hyperaldosteronism. *Circ. Res. 108*, 1417−1418.

(19) Bhave, G., Lonergan, D., Chauder, B. A., and Denton, J. S. (2010) Small-molecule modulators of inward rectifier K+ channels: recent advances and future possibilities. *Future Med. Chem. 2*, 757−774.

(20) Machida, T., Hashimoto, N., Kuwahara, I., Ogino, Y., Matsuura, J., Yamamoto, W., Itano, Y., Zamma, A., Matsumoto, R., Kamon, J., Kobayashi, T., Ishiwata, N., Yamashita, T., Ogura, T., and Nakaya, H. (2011) Effects of a highly selective acetylcholine-activated K+ channel blocker on experimental atrial fibrillation. *Circ.: Arrhythmia Electrophysiol. 4*, 94−102.

(21) Kobayashi, T., Ikeda, K., Kojima, H., Niki, H., Yano, R., Yoshioka, T., and Kumanishi, T. (1999) Ethanol opens G-protein-activated inwardly rectifying K+ channels. *Nat. Neurosci. 2*, 1091−1097.

(22) Aryal, P., Dvir, H., Choe, S., and Slesinger, P. A. (2009) A discrete alcohol pocket involved in GIRK channel activation. *Nat. Neurosci. 12*, 988−995.

(23) Yow, T. T., Pera, E., Absalom, N., Heblinski, M., Johnston, G. A., Hanrahan, J. R., and Chebib, M. (2011) Naringin directly activates inwardly rectifying potassium channels at an overlapping binding site to tertiapin-Q. *Br. J. Pharmacol. 163*, 1017−1033.

(24) Nishizawa, D., Gajya, N., and Ikeda, K. (2011) Identification of selective agonists and antagonists to g protein-activated inwardly rectifying potassium channels: candidate medicines for drug dependence and pain. *Curr. Neuropharmacol. 9*, 113−117.

(25) Niswender, C. M., Johnson, K. A., Luo, Q., Ayala, J. E., Kim, C., Conn, P. J., and Weaver, C. D. (2008) A novel assay of Gi/o-linked G protein-coupled receptor coupling to potassium channels provides new insights into the pharmacology of the group III metabotropic glutamate receptors. *Mol. Pharmacol. 73*, 1213−1224.

(26) Kennedy, J. P., Williams, L., Bridges, T. M., Daniels, R. N., Weaver, D., and Lindsley, C. W. (2008) Application of combinatorial chemistry science on modern drug discovery. *J. Comb. Chem. 10*, 345−354.

(27) Khroyan, T. V., Zhang, J., Yang, L., Zou, B., Xie, J., Pascual, C., Malik, A., Xie, J., Zaveri, N. T., Vazquez, J., Polgar, W., Toll, L., Fang, J., and Xie, X. (2012) Rodent Motor and Neuropsychological Behavior Measured in Home Cages Using the Integrated Modular Platform − SmartCage™. *Clin. Exp. Pharmacol. Physiol. 39*, 614−622.

(28) Signorini, S., Liao, Y. J., Duncan, S. A., Jan, L. Y., and Stoffel, M. (1997) Normal cerebellar development but susceptibility to seizures in mice lacking G protein-coupled, inwardly rectifying K^+ channel GIRK2. *Proc. Natl Acad. Sci. U.S.A. 94*, 923−927.